

Relationships between Clusters of Interchromatin Granules and Chromatin Fibers

Nicolas THELEN¹ and Marc THIRY²

1nthelen@uliege.be

2mthiry@uliege.be

^{1,2} Laboratory of Cell and Tissue Biology, GIGA, University of Liège, Avenue Hippocrate 15 - B 4000 Liège

Abstract

Among nuclear compartments, interchromatin granule clusters (IGCs) are widely regarded as biomolecular condensates implicated in the regulation of gene expression leading to the production of distinct mRNA species. Nevertheless, their functional dynamics within the nuclear environment remain largely elusive. In this study, we employed multiple transmission electron microscopy approaches to investigate the spatial and structural relationships between IGCs and chromatin. Our observations in HeLa cells demonstrate that IGCs establish physical connections with chromatin fibers. Furthermore, we show that the periphery of IGCs is enriched in decondensed chromatin domains and transcriptional sites. Quantitative analyses reveal that, upon α -amanitin treatment, the number of decondensed chromatin sites in proximity to IGCs is significantly reduced compared to untreated cells. In untreated conditions, a positive correlation emerges between IGC size and the abundance of adjacent decondensed chromatin regions. Based on these findings, we propose a model of IGC organization taking into account their contacts with chromatin.

Keywords : interchromatin granule cluster, nucleus, chromatin, transmission electron microscopy

Introduction

The nucleus of eukaryotic cells contains distinct functional compartments that are not delimited by membranes. These compartments appear within the nucleoplasm as biomolecular condensates, self-assembled through a thermodynamically driven liquid–liquid phase separation process (Banani et al., 2017; Giudice and Jiang, 2024; Strom and Brangwynne, 2019). The nucleolus, nuclear speckles, and Cajal bodies are well-known examples.

Nuclear speckles are highly dynamic structures (Thiry, 1995a; Tripathi and Parnaik, 2008), whose number and size vary according to cell type and physiological state. Their size increases when transcription and/or splicing is inhibited (Carmo-Fonseca et al., 1991; Carmo-Fonseca et al., 1992; Faber and Nadav-Eliyahu, 2022; Melcak et al., 2000; O’Keefe et al., 1994; Shav-Tal et al., 2001; Spector, 1993; Spector and Lamond, 2011). Under transmission electron microscopy, speckles correspond to interchromatin granule clusters (IGCs), which are composed of interconnected granules measuring 20–25 nm in diameter (Monneron and Bernhard, 1969; Puvion and Bernhard, 1975; Thiry, 1995a). Their chemical composition is characterised by an abundance of splicing factors (Carmo-Fonseca et al., 1992; Mintz et al., 1999; Misteli et al., 1997). However, numerous other molecules have also been identified within these speckles (Dopie et al., 2020), including subunits of RNA polymerase II (Xie et al., 2006), transcription factors (Alexander et al., 2025), pre-mRNA processing factors (Yoon et al., 2025), and the 20S proteasome (Baldin et al., 2008).

Currently, nuclear speckles are widely regarded as coordination platforms for mRNA regulation. They are thought to contain the molecular machinery required for transcription and pre-mRNA maturation, as well as for mRNA export and quality control (Chen and Belmont, 2019; Dias et al., 2010; Galganski et al., 2017; Gordon et al., 2021; Hall et al., 2006; Lee et al., 2022; Spector and Lamond, 2011; Tokunaga et al., 2006; Wang et al., 2018; Yoon et al., 2025). Pathologies associated with speckle dysfunction have also been reported, including Nager syndrome and craniofacial microsomia (Regan-Fendt and Izumi, 2024).

Unlike nucleoli, which contain ribosomal DNA (Thiry and Lafontaine, 2005), speckles do not appear to harbour DNA (Thiry, 1993). Nevertheless, digestion experiments using DNase I and MNase suggest that maintaining speckle structure requires association with chromatin (Raina and Rao, 2022). Furthermore, chromatin architectural factors such as cohesin and the transcriptional repressor CTCF are necessary to preserve proper speckle–chromatin interactions (Yu et al., 2025). DNA, particularly in the form of decondensed chromatin and transcriptionally active regions, has been detected within the peripheral zone surrounding IGCs (Cmarko et al., 1999; Jackson et al., 1993; Takei et al., 2021; Thiry, 1993; Wansink et al., 1993). We will refer to this peripheral compartment as the perispeckle region (Daguenet et al., 2012). The latter therefore represents a

specialised region of interchromatin spaces. It extends from the outer surface of the IGCs to the clumps of condensed chromatin located around their periphery.

In this work, we examined the interplay between chromatin and IGCs in HeLa cells treated or untreated with α -amanitin, an inhibitor of RNA polymerase II transcription. We first assessed the impact of transcriptional inhibition on the three-dimensional structure of IGCs using confocal microscopy, followed by three complementary transmission electron microscopy techniques. The cytochemical acetylation method was employed to enhance the contrast of condensed chromatin near IGCs. In addition, immunogold detection of modified nucleotides added to DNA termini by a specific transferase on ultrathin sections enabled the identification of decondensed DNA in the immediate vicinity of IGCs. Finally, we investigated RNA synthesis sites at the ultrastructural level by incorporating BrUTP into cells via a transfection vector. This work was supplemented by quantitative and statistical analysis of the data obtained for each ultrastructural approach used to better understand the significance of the differences observed between different cellular compartments under the same experimental condition or between the same cellular compartment under different experimental conditions. Our findings clearly indicate that chromatin fibres connect IGCs within the nucleus. Although chromatin clumps persist at the periphery of large IGCs in α -amanitin-treated cells, quantitative analysis reveals that the number of decondensed DNA sites adjacent to IGCs is higher in untreated cells. In these cells, the larger the IGC, the greater the number of decondensed DNA sites. We also confirm that RNA synthesis sites are in the perispeckle region. Ultimately, we propose a dynamic model of IGC organisation within the nucleus based on their interactions with chromatin.

Materials and Methods

Biological Materials

HeLa cells were cultured at 37 °C under 5% CO₂ in Dulbecco's Modified Eagle Medium (Gibco-BRL, Life Technologies, Ghent, Belgium) supplemented with 10% fetal calf serum and 100 U/ml penicillin. For transcriptional inhibition, selected cultures were treated for 3 h with 10 µg/ml α-amanitin (Sigma, St. Louis, USA), a concentration known to inhibit polymerase II without affecting polymerase I in HeLa cells (Pombo et al., 1999).

Immunofluorescence Procedures

Slides were fixed for 10 min at room temperature in 4% formaldehyde (Ladd research, USA) prepared in 0.1 M PBS (pH 7.4), rinsed twice for 10 min in PBS, and permeabilized for 6 min in 0.5% Triton X-100 (Thermo Fischer Scientific, Belgium). Subsequently, they were washed in PBS containing 1% BSA (w/v, Sigma) and normal rabbit serum (NRS, Sigma) diluted 1:30, followed by incubation for 60 min at 37 °C with anti-mouse SC35 antibodies (Sigma) diluted 1:2000 in PBS supplemented with NRS (1:50) and 0.2% BSA. After three washes in PBS containing 1% BSA (10 min each), slides were incubated for 60 min at 37 °C with Alexa Fluor 594 rabbit anti-mouse antibody (Molecular Probes) diluted 1:2000 in PBS containing 0.2% BSA. Following rinsing, slides were counterstained for 15 min at room temperature with Hoechst 33258 (1:500, Sigma), rinsed in distilled water, and mounted using CitiFluor™ AF1 (Agar Scientific, Stansted, UK).

Confocal Microscopy and Three-Dimensional Reconstructions

A Bio-Rad 1024ES system (Bio-Rad, Hercules, CA, USA) mounted on an inverted Olympus IX70 microscope was employed. Image acquisition was performed using a 60× plan-apochromat oil immersion objective (NA = 1.4). FITC was excited with the 488 nm line of a Krypton/Argon laser, and emission was collected through a 522 ± 16 nm band-pass filter. Phase-contrast images were simultaneously recorded on a dedicated detector. For 3D analysis, 30–50 optical sections were captured from the top of the cell at 0.5 µm z-steps and reconstructed as previously described (Heliot et al., 1997). Surface rendering was subsequently applied (Cheutin et al., 2002).

Transmission Electron Microscopy

Cells were fixed for 60 min at 4 °C in 1.6% glutaraldehyde (Ladd Research) in 0.1 M Sorensen's buffer (pH 7.4) and acetylated as previously reported (Thiry et al., 1985). After washing in Sorensen's buffer, samples were dehydrated through graded ethanol series and embedded in Epon (Laborimpex, Belgium). Ultrathin sections were mounted

on collodion-coated grids and stained with uranyl acetate (Fluka, Switzerland) and lead citrate (Sigma) prior to examination in a JEM 1400 transmission electron microscope operating at 80 kV. Random fields were photographed using an 11-megapixel camera system (Quemesa, Olympus).

Detection of DNA: In Situ Terminal Deoxynucleotidyl Transferase (TdT) Immunogold Method

The TdT-based immunogold technique was applied as previously described (Thiry, 1992). Acetylated ultrathin sections were incubated for 30 min at 37 °C in a reaction medium containing 100 mM sodium cacodylate (pH 6.5), 10 mM β -mercaptoethanol (Janssen Chimica, Belgium), 2 mM $MnCl_2$ (Sigma), 50 μ g/ml BSA, 20 μ M 5-bromo-2'-deoxyuridine triphosphate (BUdR, Sigma), 4 μ M each of dCTP, dGTP, and dATP (Boehringer Mannheim, Germany), and 125 U/ml TdT (Boehringer Mannheim). After rinsing, sections were blocked with normal goat serum (NGS) and incubated for 4 h at room temperature with mouse anti-BUdR antibodies (Roche) diluted 1:50 in PBS containing 0.2% BSA and NGS. Detection was achieved using rabbit anti-mouse IgG conjugated to 10 nm colloidal gold particles (Amersham Life Science) diluted 1:40. Control experiments omitting either TdT or the primary antibody yielded no detectable labelling.

Between 22 and 42 micrographs per sample were acquired at magnifications ranging from 10,000 \times to 15,000 \times in randomly selected nuclear regions. Morphometric analyses were performed using iTEM 5.2 software (Olympus SIS).

A t-student test was applied to determine the significance of the differences in labelling levels obtained between the nuclear compartments and the resin and/or cytoplasm in each condition. In addition, a Pearson test was used to study the relationship between the size of the IGCs and the labelling observed in the perispeckles region. The outer boundary of the IGCs in the micrographs is visually defined based on the presence of granules.

Detection of Newly Synthesised RNA

Transfection reagents used for BrUTP (Sigma) incorporation in HeLa cells were FuGene-6 (Roche). We used a protocol described previously and incubated the cells for 15 minutes in culture medium without the complex after lipofection, a time that allows nascent RNAs to be identified (Thiry et al., 2008). Immunolabelling after BrUTP incorporation, each well was fixed for 10 min at room temperature in 2% formaldehyde in buffered PBS (pH 7.4) and washed three times with PBS. A solution of Triton X-100 0.3% in PBS was added to each well for 15 min followed by three washes of PBS. The preparation was blocked by normal goat serum (NGS, Sigma) diluted 1/20 in PBS and

then indirectly immunolabelled for 30 min at 37 °C by mouse anti-BUdR antibodies (Roche, USA) diluted 1/100 in PBS (pH 7.2). The staining was revealed during 30 min at 37 °C by secondary goat anti-mouse coupled to 10 nm gold particles and diluted 1/40 in PBS. Several kinds of control experiments were carried out. First, BrUTP were omitted from the incorporation step and in second control, the primary antibody was omitted. In both cases, no labelling was observed.

Between 20 and 12 micrographs of each sample were taken at different magnifications (from 13,000 x to 20,000 x) in randomly selected regions to provide a morphological description. Morphometric measurements were performed and analysed as described above. A t-student test was applied to determine the significance of the differences in labelling levels obtained between the nuclear compartments and the cytoplasm in each condition.

Results

Confocal Microscopy

To confirm that α -amanitin treatment induces the formation of enlarged speckles in HeLa cells, we first performed confocal microscopy using SC35, a well-established marker of nuclear speckles. Analysis of optical sections revealed that, in α -amanitin-treated cells, certain SC35-labelled foci were markedly larger than those observed in untreated cells. In addition, an alignment of multiple SC35 clusters forming chain-like structures was occasionally detected. Surface rendering of SC35-labelled speckles in untreated cells showed that these clusters were generally spherical (Fig. 1A), although their surfaces appeared irregular and spiculated. The clusters were spatially separated and located in regions exhibiting weak Hoechst staining. Both the size and number of SC35 foci per nucleus varied among cells. In contrast, surface rendering of α -amanitin-treated cells revealed that some clusters had lost their spherical morphology, adopting elongated shapes (Fig. 1B, arrowheads), possibly resulting from the fusion of multiple speckles. Their surfaces appeared more irregular and spiny compared to untreated cells. The total volume occupied by the IGCs represents approximately 5% of the nuclear volume under control conditions. It is 4% in cells treated with α -amanitin.

Using confocal microscopy and 3D reconstruction of the images obtained, we confirm that treatment with α -amanitin induces a reorganisation of IGCs in the nucleus of HeLa cells, particularly the frequent formation of elongated IGCs.

Transmission Electron Microscopy

Cytochemical Acetylation Method

To investigate the spatial relationship between chromatin and IGCs, we first applied the cytochemical acetylation method to both untreated and α -amanitin-treated cells. This technique enhances the contrast of condensed chromatin within the nucleus, thereby improving its visualisation in RNP-rich compartments.

In untreated cells, IGCs appeared as rounded structures with an average area of approximately $0.33 \pm 0.16 \mu\text{m}^2$ ($n = 42$), composed of numerous small granules (Fig. 2A). The peripheral zone of IGCs contained clumps of condensed chromatin. These clumps did not establish direct contact with the IGCs; rather, only certain chromatin fibres extended from these clumps into the intervening space, occasionally reaching the outer IGC surface (Figs. 2A, 2B).

In α -amanitin-treated cells (Fig. 2C), enlarged IGCs were observed in 75% of the examined nuclei ($n = 100$), with an average area of approximately $0.62 \pm 0.21 \mu\text{m}^2$ ($n = 25$). A Student's t-test confirmed that this difference in mean area between conditions was statistically significant ($p < 0.001$). These enlarged IGCs were also composed of

numerous granules, but their density was higher in the central region than at the periphery (Fig. 2D). The average area of the perispeckles is $0.24 \pm 0.05 \mu\text{m}^2$ ($n=25$). A Student's t-test indicates that the observed difference between the mean areas of the IGCs under the two conditions is significant ($p < 0.01$). The thickness of the perispeckles ranges from 10 to 325 nm.

Using the cytochemical method of acetylation, we confirmed the presence of decondensed chromatin fibres in the perispeckle region, but we are showing for the first time direct contact of some fibers with the outer surface of IGCs. Statistical analysis also shows that their frequency is higher in untreated cells.

Immunocytochemical Detection of DNA Using TdT

Because the acetylation method does not allow identification of decondensed chromatin, we next employed the TdT-based immunogold technique to localise DNA with high sensitivity, regardless of its condensation state (Thiry and Daneholt, 1998). This method was applied to ultrathin sections previously processed by acetylation.

In untreated cells (Fig. 3A), gold particles were predominantly associated with condensed chromatin blocks, with lighter labelling observed on decondensed chromatin within interchromatin spaces. Virtually no labelling was detected within IGCs. However, in the perispeckles—particularly near the IGC surface—gold particles were clearly present on decondensed chromatin.

A similar distribution was observed in α -amanitin-treated cells (Fig. 3B), although the density of gold particles in the perispeckles appeared reduced. Quantitatively, 93% of IGCs in untreated cells exhibited labelling in the perispeckles region, compared to 76% in treated cells.

Statistical analysis (Fig. 4) confirmed that labelling over condensed chromatin and in the periphery of IGCs was significantly higher than background (resin or cytoplasm) in both conditions, whereas labelling within IGCs was not significant. A Student's t-test further demonstrated that the difference in labelling in the perispeckles region between untreated and treated cells was highly significant ($p < 0.001$).

We also examined whether the number of gold particles in the perispeckles correlated with IGC size. In untreated cells (Fig. 5A), a positive correlation was observed (Pearson correlation coefficient: 0.6), indicating that larger IGCs were associated with more decondensed chromatin contacts. In contrast, no such correlation was detected in treated cells (Pearson coefficient: -0.2), and the trend even appeared reversed (Fig. 5B).

Using an immunocytological approach involving DNA end elongation by a specific transferase, we confirm the presence of DNA in the perispeckle region. No labelling is observed in the IGCs themselves. Furthermore, additional statistical analysis of the

labelling observed shows for the first time that the presence of DNA in the perispeckle region is higher in untreated cells and that in these cells the size of the IGCs is large.

Localisation of RNA Synthesis Sites Using BrUTP Incorporation

To map RNA synthesis sites in the vicinity of IGCs, cells were transiently transfected with BrUTP–FuGene complexes, and incorporated BrUTP was detected by immunogold labelling.

In untreated cells, gold particles were localised within the fibrillar components of the nucleolus and in interchromatin spaces adjacent to condensed chromatin blocks (Fig. 6A). Notably, clear labelling was observed in the perispeckle region, whereas no signal was detected within the IGCs themselves.

In α -amanitin-treated cells (Fig. 6B), only a few gold particles were detected in nucleolar fibrillar components and interchromatin spaces, and no labelling was observed either within IGCs or in the perispeckles.

A quantitative study was conducted to assess the significance of the labeling obtained using this approach (Fig. 7). A Student's t-test indicates significant labeling in the fibrillar components of the nucleolus compared to that observed in the cytoplasm, both in untreated cells and in cells treated with α -amanitin ($p < 0.001$). In control cells, labeling of the perispeckles is also significant ($p < 0.001$). In contrast, labeling of condensed chromatin and IGCs is not significant under either condition.

Using a recent technique for detecting nascent RNAs, we confirm the presence of newly synthesised RNAs in the perispeckle region. No labelling is observed in the IGCs themselves.

Discussion

Our ultrastructural analysis strongly supports preferential contacts between interchromatin granule clusters (IGCs) and chromatin. More specifically, we demonstrate that these interactions involve decondensed chromatin regions that establish direct contact with the IGC surface, whereas no DNA was detected within the IGCs themselves—a finding fully consistent with earlier ultrastructural observations (Thiry, 1993).

The presence of decondensed chromatin in the perispeckles surrounding IGCs strongly suggests that these interactions play a critical role in the functional organisation of nuclear speckles. This interpretation is reinforced by recent biochemical studies showing that speckle–chromatin associations are essential for maintaining speckle integrity (Raina and Rao, 2022) and that chromatin architectural proteins such as cohesin and CTCF are required to stabilise these associations (Yu et al., 2025). Nevertheless, the precise molecular nature of these interactions remains poorly understood.

Our quantitative data further reveal that the number of chromatin contacts varies according to the transcriptional state of the cell. In untreated cells, a positive correlation exists between IGC size and the number of peripheral decondensed chromatin sites, suggesting that transcriptional activity promotes the recruitment of chromatin regions to IGCs. In contrast, this correlation disappears—and even reverses—under α -amanitin treatment, which inhibits RNA polymerase II transcription. These findings imply that transcriptional inhibition triggers the coalescence of IGCs into larger, non-functional aggregates, a phenomenon reminiscent of the giant IGCs observed during early mitosis when transcription is globally silenced (Thiry, 1995b). Similar morphological changes have also been reported following treatment with camptothecin (Elias et al., 2003) and DRB (Melcak et al., 2000).

We also observed that α -amanitin-treated IGCs frequently exhibit a denser central region and a less compact periphery. This structural rearrangement has previously been described during early mitosis (Thiry, 1995b). The presence of more densely packed granules within the IGC may indicate a slowdown in the activity of this nuclear structure. Further studies are needed to determine their function. However, it should not be confused with the subcompartmentalisation of speckles reported by super-resolution microscopy (Dopie et al., 2020). At the ultrastructural level, IGCs appear as highly homogeneous assemblies of numerous granules, and the two-zone organisation inferred from confocal imaging is not discernible (Fei et al., 2017). Nevertheless, the

presence of IGC extensions toward decondensed chromatin in untreated cells may represent the structural basis for specialised functional domains within speckles.

Based on our results, we propose a dynamic model of IGC organization within the cell nucleus (Fig. 8). The activation of genes leads to the recruitment of the entire machinery required for their expression, notably the splicing apparatus. The pooling of all this material recruited by multiple genes results in highly organized structures, whose core corresponds to an IGC, while the perispeckle could represent sites where certain transcriptionally active genes interact with IGCs. Indeed, we have shown in this study and in a previous one (Thiry, 1993) that these perispeckles contain decondensed chromatin. Here, we reveal that this chromatin comes into contact with the IGCs.

This model aligns with optical microscopy studies suggesting that transcription occurs at the periphery of speckles (Barutcu et al., 2022; Hall et al., 2006; Johnson et al., 2000; Kim et al., 2019; Su et al., 2020; Takei et al., 2021) and corroborates earlier electron microscopy findings indicating that RNA synthesis sites are located around IGCs (Cmarko et al., 1999). Our BrUTP incorporation experiments further confirm that the perispeckle region harbours active transcription sites under normal conditions, whereas these sites disappear upon transcriptional inhibition.

Moreover, the perispeckle region has been identified by correlative microscopy as a major assembly site for exon junction complexes (Daguenet et al., 2012). The size of this functional domain likely reflects the number of active genes engaged in transcription. Consequently, a reduction in transcriptional activity—whether physiologically during mitotic entry or experimentally through chemical inhibitors such as α -amanitin— could release IGCs from their interaction with chromatin fibers , allowing them to coalesce into large, transcriptionally inert aggregates within the nucleus.

Collectively, these findings provide new mechanistic insights into the interplay between nuclear speckles and chromatin, highlighting their dynamic reorganisation in response to transcriptional cues and reinforcing the view that IGCs act as central hubs coordinating gene expression within the three-dimensional nuclear architecture. However, the effects observed with α -amanitin (nuclear reorganisation, IGC enlargement and fusion) could reflect general architectural changes rather than IGC-specific consequences.

References

- Alexander, K.A., Yu, R., Skuli, N., Coffey, N.J., Nguyen, S, Faunce, C.L., Huang, H., Dardani, I.P., Good, A.L., Lim, J., Li, C.Y., Biddle, N., Joyce, E.F., Raj, A., Lee, D., Keith, B., Simon, M.C., Berger, S.L. (2025) Nuclear speckles regulate functional programs in cancer. *Nat. Cell Biol.* 27(2), 322-335.
- Baldin, V., Militello, M., Thomas, Y., Doucet, C., Fic, W., Boireau, S., Jariel-Encontre, I., Piechaczyk, M., Bertrand, E., Tazi, J., Coux, O. (2008) A novel role for PA28gamma-proteasome in nuclear speckle organization and SR protein trafficking. *Mol. Biol. Cell* 19(4),1706-1716.
- Banani, S.F., Lee, H.O., Hyman, A.A. and Rosen, M.K. (2017) Biomolecular condensates: organizers of cellular biochemistry. *Nat. Rev. Mol. Cell Biol.* 18, 285-298.
- Barutcu, A.R., Wu, M., Braunschweig, U., Dyakov, B.J.A., Luo, Z., Turner, K. M., Durbic, T., Lin, Z. Y., Weatheritt, R.J., Maass, P.G., Gingras A.C., Blencowe B.J. (2022) Systematic mapping of nuclear domain-associated transcripts reveals speckles and lamina as hubs of functionally distinct retained introns. *Mol. Cell* 82, 1035-1052.
- Carmo-Fonseca, M., Tollervey, D., Pepperkok, R., Barabino, S. M., Merdes, A., Brunner, C., Zamore, P.D., Green, M.R., Hurt, E., Lamond, A.I. (1991) Mammalian nuclei contain foci which are highly enriched in components of the pre-mRNA splicing machinery. *EMBO J.* 10, 195-206.
- Carmo-Fonseca, M., Pepperkok, R., Carvalho, M.T., Lamond, A.I. (1992) Transcription-dependent colocalization of the U1, U2, U4/U6, and U5 snRNPs in coiled bodies. *J Cell Biol.* 117(1),1-14.
- Chen, Y., Belmont, A.S. (2019) Genome organization around nuclear speckles. *Curr. Opin. Genet. Dev.* 55, 91-99.
- Cheutin, T., O'Donohue, M.-F., Beorchia, A., Vandelaer, M., Kaplan, H., Deféver, B., Ploton, D., Thiry, M. (2002) Three-dimensional organization of active rRNA genes within the nucleolus. *J. Cell Sci.* 115, 3297-3307.
- Cmarko, D., Verschure, P.J., Martin, T.E., Dahmus, M.E., Krause, S., Fu, X.D., van Driel, R., Fakan, S. (1999) Ultrastructural analysis of transcription and splicing in the cell nucleus after bromo-UTP microinjection. *Mol. Biol. Cell* 10, 211–223.
- Daguenet, E., Baguet, A., Degot, S., Schmidt, U., Alpy, F., Wendling, C., Spiegelhalter, C., Kessler, P., Rio, M.C., Le Hir, H., Bertrand, E., Tomasetto, C. (2012) Perispeckles are major assembly sites for the exon junction core complex. *Mol. Biol. Cell* 23(9),1765-1782.
- Dias, A.P., Dufu, K., Lei, H., Reed, R. (2010) A role for TREX components in the release of spliced mRNA from nuclear speckle domains. *Nat. Commun.* 19, 1: 97.

Dopie, J., Sweredoski, M.J., Moradian, A., Belmont, A.S. (2020) Tyramide signal amplification mass spectrometry (TSA-MS) ratio identifies nuclear speckle proteins. *J. Cell Biol.* 219(9), e201910207.

Elias, E., Lalun, N., Lorenzato, M., Blache, L., Chelidze, P., O'Donohue, M.F., Ploton, D., Bobichon, H. (2003) Cell-cycle-dependent three-dimensional redistribution of nuclear proteins, P 120, pKi-67, and SC 35 splicing factor, in the presence of the topoisomerase I inhibitor camptothecin. *Exp. Cell Res.* 291(1), 176-188.

Faber, G.P., Nadav-Eliyahu S, Shav-Tal Y. 2022. Nuclear speckles - a driving force in gene expression. *J Cell Sci.* Jul 1;135(13): jcs259594.

Fei, J., Jadalaha, M., Harmon, T.S., Li, I.T.S., Hua, B., Hao, Q., Holehouse, A.S., Reyer, M., Sun, Q., Freier, S.M., Pappu, R.V., Prasanth, K.V., Ha, T. (2017) Quantitative analysis of multilayer organization of proteins and RNA in nuclear speckles at super resolution. *J. Cell Sci.* 130(24), 4180-4192.

Galganski, L., Urbanek, M.O., Krzyzosiak, W.J. (2017) Nuclear speckles: molecular organization, biological function and role in disease. *Nucleic Acids Res.* 45(18),10350-10368.

Giudice, J., Jiang, H. (2024) Splicing regulation through biomolecular condensates and membraneless organelles. *Nat. Rev. Mol. Cell Biol.* 25(9), 683-700.

Gordon, J.M., Phizicky, D.V., Neugebauer, K.M. (2021) Nuclear mechanisms of gene expression control : pre-mRNA splicing as a life or death decision. *Curr. Opin. Genet. Dev.* 67, 67-76.

Hall, L.L., Smith, K.P., Byron, M., Lawrence, J.B. (2006) Molecular anatomy of a speckle. *Anat. Rec. A Discov. Mol. Cell Evol. Biol.* 288, 664–675.

Heliot, L., Kaplan, H., Lucas, L., Klein, C., Beorchia, A., Doco-Fenzy, M., Menager, M., Thiry, M., O'Donohue, M.-F., Ploton, D. (1997) Electron tomography of metaphase nucleolar organizer regions: evidence for a twisted-loop organization. *Mol. Biol. Cell* 8, 2199-2216.

Jackson, D.A., Hassan, A.B., Errington, R.J., Cook, P.R. (1993) Visualization of focal sites of transcription within human nuclei *EMBO J.* 12(3),1059-1065.

Johnson, C., Primorac, D., McKinstry, M., McNeil, J., Rowe, D., Lawrence, J.B. (2000) Tracking COL1A1 RNA in osteogenesis imperfecta. splice-defective transcripts initiate transport from the gene but are retained within the SC35 domain. *J. Cell Biol.* 150, 417–432.

Kim, J., Han, K. Y., Khanna, N., Ha, T., Belmont, A.S. (2019) Nuclear speckle fusion via long-range directional motion regulates speckle morphology after transcriptional inhibition. *J. Cell Sci.* 132, jcs226563.

Lee, E.S., Smith, H.W., Wolf, E.J., Guvenek, A., Wang, Y.E., Emili, A., Tian, B., Palazzo, A.F. (2022) ZFC3H1 and U1-70K promote the nuclear retention of mRNAs with 5' splice site motifs within nuclear speckles. *RNA* 28(6), 878-894.

Melcak, I., Cermanova, S., Jirsova, K., Koberna, K., Malinsky, J., Raska, I. (2000) Nuclear pre-mRNA compartmentalization: Trafficking of released transcripts to splicing factor reservoirs. *Mol. Biol. Cell* 11, 497–510.

Mintz, P.J., Patterson, S.D., Neuwald, A.F., Spahr, C.S., Spector, D.L. (1999) Purification and biochemical characterization of interchromatin granule clusters. *EMBO J.* 18, 4308–4320.

Misteli, T., Cáceres, J.F., Spector, D.L. (1997) The dynamics of a pre-mRNA splicing factor in living cells. *Nature* 387, 523–527.

Monneron, A., Bernhard, W. (1969) Fine structural organization of the interphase nucleus in some mammalian cells. *J. Ultrastruct. Res.* 27, 266–288.

O’Keefe, R.T., Mayeda, A., Sadowski, C.L., Krainer, A.R., Spector, D.L. (1994) Disruption of pre-mRNA splicing in-vivo results in reorganization of splicing factors. *J. Cell Biol.* 124, 249–260.

Pombo, A., Jackson, D.A., Hollinshead, M., Wang, Z., Roeder, R.G., Cook, P.R. (1999) [Regional specialization in human nuclei: visualization of discrete sites of transcription by RNA polymerase III.](#) *EMBO J.* 18(8), 2241-2253.

Puvion, E., Bernhard, W. (1975) Ribonucleoprotein components in liver cell nuclei as visualized by cryoultramicrotomy. *J. Cell Biol.* 67(1), 200-214.

Raina, K., Rao, B.J., 2022, Mammalian nuclear speckles exhibit stable association with chromatin: a biochemical study. *Nucleus* 13(1), 58-73.

Regan-Fendt, K.E., Izumi, K. (2024) Nuclear speckleopathies: developmental disorders caused by variants in genes encoding nuclear speckle proteins. *Hum. Genet.* 143(4), 529-544.

Shav-Tal, Y., Lee, B. C., Bar-Haim, S., Schori, H., Zipori, D. (2001) Reorganization of nuclear factors during myeloid differentiation. *J. Cell. Biochem.* 81, 379-392.

Spector, D.L. (1993) Macromolecular domains within the cell nucleus. *Annu. Rev. Cell Biol.* 9, 265–315.

Spector, D.L., Lamond, A.I. (2011) Nuclear speckles. *Cold Spring Harb Perspect Biol.* 3(2), a000646.

Strom, A.R., Brangwynne, C.P. (2019) The liquid nucleome - phase transitions in the nucleus at a glance. *J. Cell Sci.* 132, jcs235093.

- Su, J.H., Zheng, P., Kinrot, S.S., Bintu, B., Zhuang, X. (2020) Genome-scale imaging of the 3D organization and transcriptional activity of chromatin. *Cell* 182, 1641-1659.
- Takei, Y., Yun, J., Zheng, S., Ollikainen, N., Pierson, N., White, J., Shah, S., Thomassie, J., Suo, S., Eng, C. L., Guttman, M., Yuan, G.C., Cai, L. (2021) Integrated spatial genomics reveals global architecture of single nuclei. *Nature* 590, 344-350.
- Thiry, M. (1992) Highly sensitive immunodetection of DNA on sections with exogenous terminal deoxynucleotidyl transferase and non-isotopic nucleotide analogues. *J. Histochem. Cytochem.* 40 (3), 411-419.
- Thiry, M. (1993) Differential location of nucleic acids within interchromatin granule clusters. *Eur. J. Cell Biol.* 62(2), 259-269.
- Thiry, M. (1995a) Behavior of interchromatin granules during the cell cycle. *Eur. J. Cell Biol.* 68(1), 14-24.
- Thiry, M. (1995b) The interchromatin granules. *Histol. Histopathol.* 10, 1035-1045.
- Thiry, M., Lepoint, A., Goessens, G. (1985) Re-evaluation of the site of transcription in Ehrlich tumour cell nucleoli. *Biol Cell* 54(1), 57-64.
- Thiry, M., Lamaye, F., Thelen, N., Chatron-Colliet, A., Lalun, N., Bobichon, H., Ploton, D. (2008) A protocol for studying the kinetics of RNA within cultured cells: application to ribosomal RNA. *Nat. Protoc.* 3, 1997-2004.
- Thiry, M., Daneholt, B. (1998) Evaluation of the sensitivity of the terminal deoxynucleotidyl transferase immunogold technique on Balbani ring genes. *J. Histochem. Cytochem.* 46 (3), 345-351.
- Thiry, M., Lafontaine, D.L.J. (2005) Birth of a nucleolus: the evolution of nucleolar compartments. *Trends Cell Biol.*, 15 (4), 194-199.
- Tokunaga, K., Shibuya, T., Ishihama, Y., Tadakuma, H., Ide, M., Yoshida, M., Funatsu, T., Ohshima, Y., Tani, T. (2006) Nucleocytoplasmic transport of fluorescent mRNA in living mammalian cells: nuclear mRNA export is coupled to ongoing gene transcription. *Genes Cells* 11(3), 305-17.
- Tripathi, K., Parnaik, V.K. (2008) Differential dynamics of splicing factor SC35 during the cell cycle. *J. Biosci.* 33(3), 345-354.
- Wang, K., Wang, L., Wang, J., Chen, S., Shi, M., Cheng, H. (2018) Intronless mRNAs transit through nuclear speckles to gain export competence. *J. Cell Biol.* 217, 3912-3929.
- Wansink, D.G., Schul, W., van der Kraan, I., van Steensel, B., van Driel, R., de Jong, L. (1993) Fluorescent labeling of nascent RNA reveals transcription by RNA polymerase II in domains scattered throughout the nucleus. *J Cell Biol.* 122, 283-293.

Xie, S.Q., Martin, S., Guillot, P.V., Bentley, D.L., Pombo, A. (2006) Splicing speckles are not reservoirs of RNA polymerase II, but contain an inactive form, phosphorylated on serine2 residues of the C-terminal domain. *Mol. Biol. Cell* 17(4), 1723-1733.

Yoon, Y., Bournique, E., Soles, L.V., Yin, H., Chu, H.F., Yin, C., Zhuang, Y., Liu, X., Liu, L., Jeong, J., Yu, C., Valdez, M., Tian, L., Huang, L., Shi, X., Seelig, G., Ding, F., Tong, L., Buisson, R., Shi, Y. (2025) RBBP6 anchors pre-mRNA 3' end processing to nuclear speckles for efficient gene expression. *Mol. Cell* 85(3), 555-570.

Yu, R., Roseman, S., Siegenfeld, A.P., Gardner, Z., Nguyen, S.C., Tran, K.A., Joyce, E.F., Jain, R., Liao, B.B., Krantz, I.D., Alexander, K.A., Berger, S.L. (2025) CTCF/RAD21 organize the ground state of chromatin-nuclear speckle association. *Nat. Struct. Mol. Biol.* 32(6), 1069-1080.

Figure Legends

Fig. 1 Three-dimensional reconstruction and surface rendering of a HeLa cell nucleus either untreated (a) or treated with α -amanitin (b). Optical sectioning through the DNA volume (blue) enabled visualisation of SC35-labelled speckles (red) within the nuclear space. Arrowheads indicate elongated IGC. Scale bar: 5 μ m.

Fig. 2 Visualisation of condensed chromatin (C) revealed by the cytochemical acetylation method in HeLa cell nuclei, either untreated (a, b) or treated with α -amanitin (c, d). IGCs are delineated by dashed lines. Small blocks of condensed chromatin are observed in close proximity to IGCs (large arrowheads), while fibres extending from these blocks occasionally reach the IGC surface (small arrowheads). The perispeckles (P) are areas extending from the dotted line to the dashed line connecting the various clumps of condensed chromatin bordering the IGCs. In treated cells, the IGC core frequently appears denser (interrupted line, d). Scale bar: 0.2 μ m.

Fig. 3 Detection of DNA by the TdT immunogold technique in HeLa cell nuclei, either untreated (a) or treated with α -amanitin (b). IGCs are outlined by dashed lines. Gold particles associated with non-condensed chromatin (C) are detected in the immediate periphery of IGCs (arrows). Rare gold particles are present within IGCs (circle). Scale bar: 0.2 μ m.

Fig. 4 Mean densities of gold particles (number of particles per square micrometre) across different nuclear compartments in HeLa cells, untreated or treated with α -amanitin for 3 h. The values obtained for the different cellular compartments in untreated or treated cells are as follows: Resin: 1.02 ± 0.6 (n=22)/ 0.83 ± 0.47 (n=23) ; Cytoplasm: 1.65 ± 0.99 (n=30)/ 2.08 ± 1.74 (n=22) ; Condensed chromatin: 170.43 ± 28.84 (n=31)/ 201.24 ± 36.72 (n=22) ; IGC: 0.6 ± 1.42 (n=42)/ 1.47 ± 1.44 (n=25) ; Perispeckle: 7.43 ± 4.14 (n=38)/ 5.66 ± 4.85 (n=25).

Fig. 5 Trend curves illustrating the relationship between IGC area and the number of gold particles located in their periphery in untreated (a) and α -amanitin-treated (b) HeLa cells.

Fig. 6 Detection of newly synthesised RNA in HeLa cells transfected for 15 min with BrUTP–FuGene complexes prior to fixation. BrUTP-labelled RNA was visualised by indirect immunogold labelling. IGCs are outlined by dashed lines. In untreated cells (a), strong labelling is observed in the periphery of IGCs (arrows). In contrast, no peripheral labelling is detected in α -amanitin-treated cells (b). A few gold particles are present in the nucleolus (Nu). C: condensed chromatin; NE: nuclear envelope. Scale bar: 0.2 μ m.

Fig. 7 Mean densities of gold particles (number of particles per square micrometer) over the different cellular compartments in HeLa cells non-treated or treated with α -amanitin for 3 hr and transfected with BrUTP/fugene complexes for 15 min.

Fig. 8 Dynamic model for IGC organization. IGC organization in α -amanitin-untreated (left) and α -amanitin-treated (right). See text for description.

Figure 1

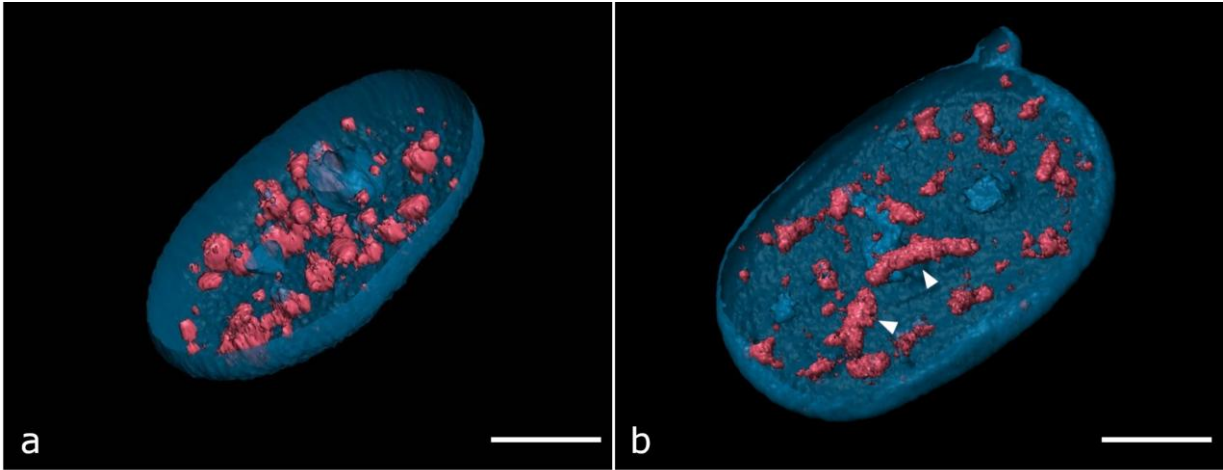


Figure 2

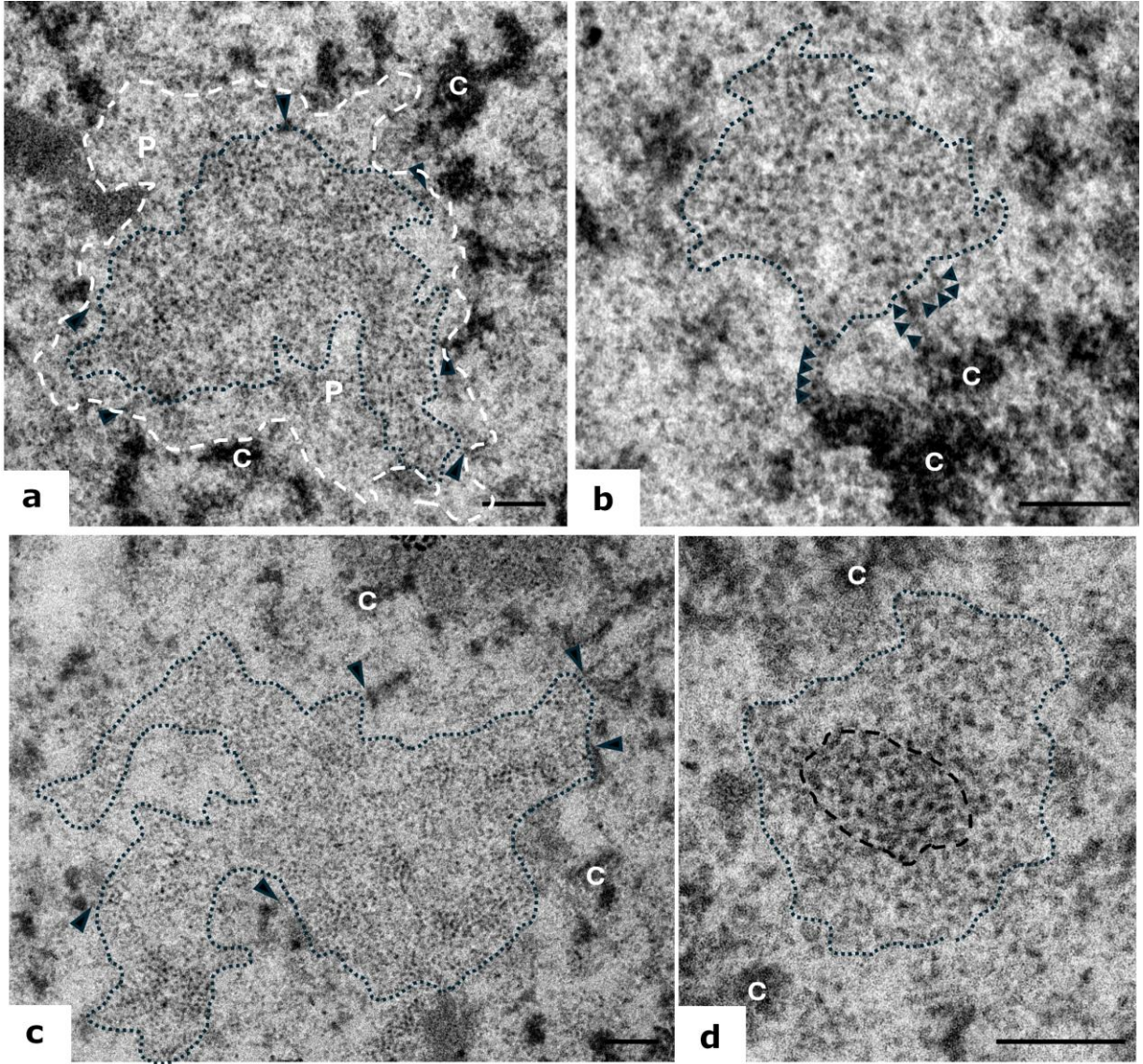


Figure 3

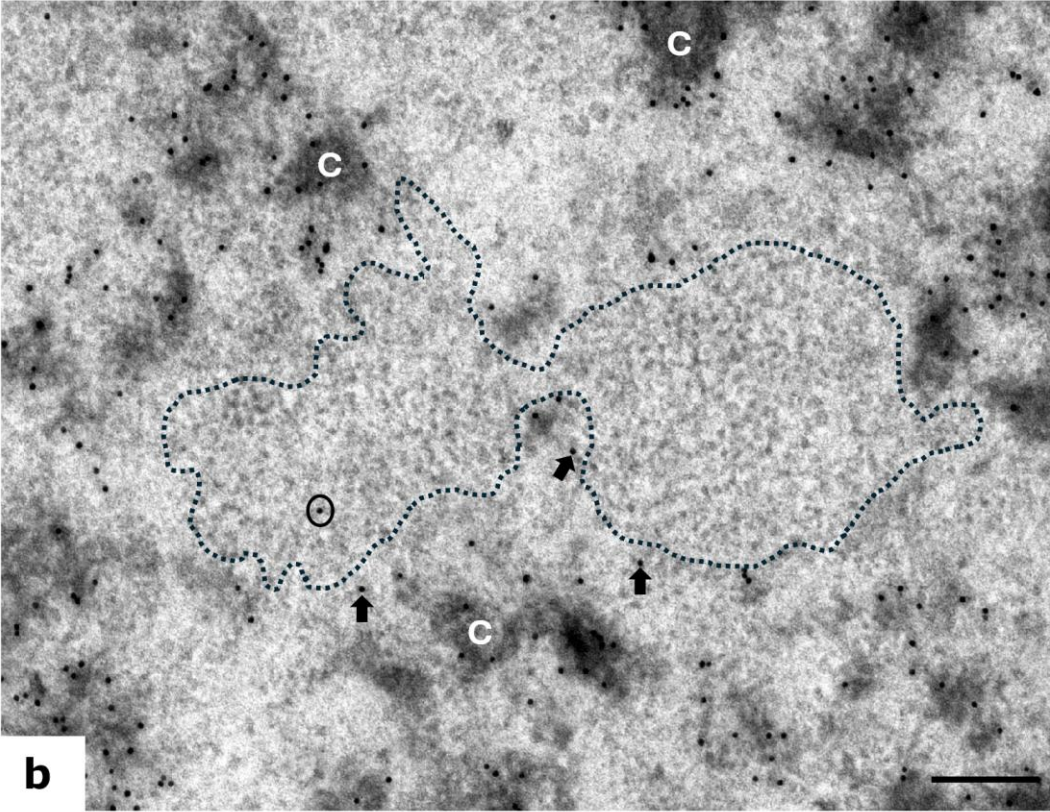
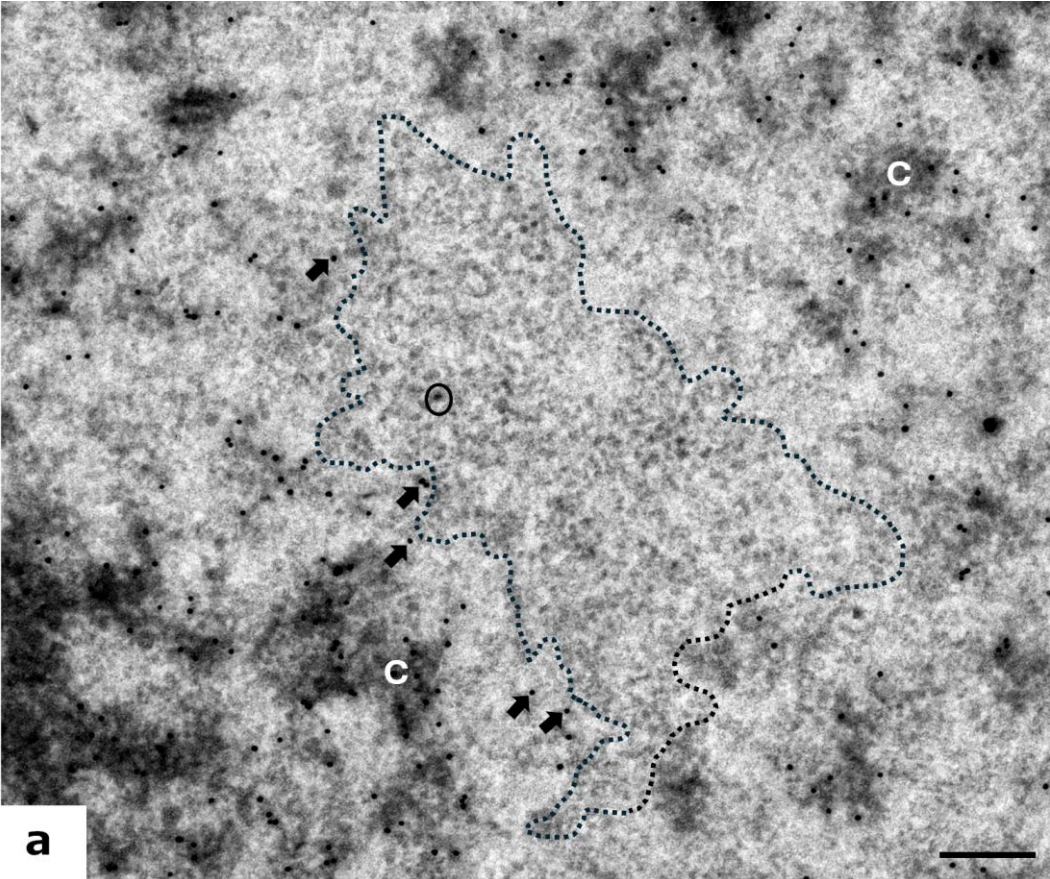


Figure 4

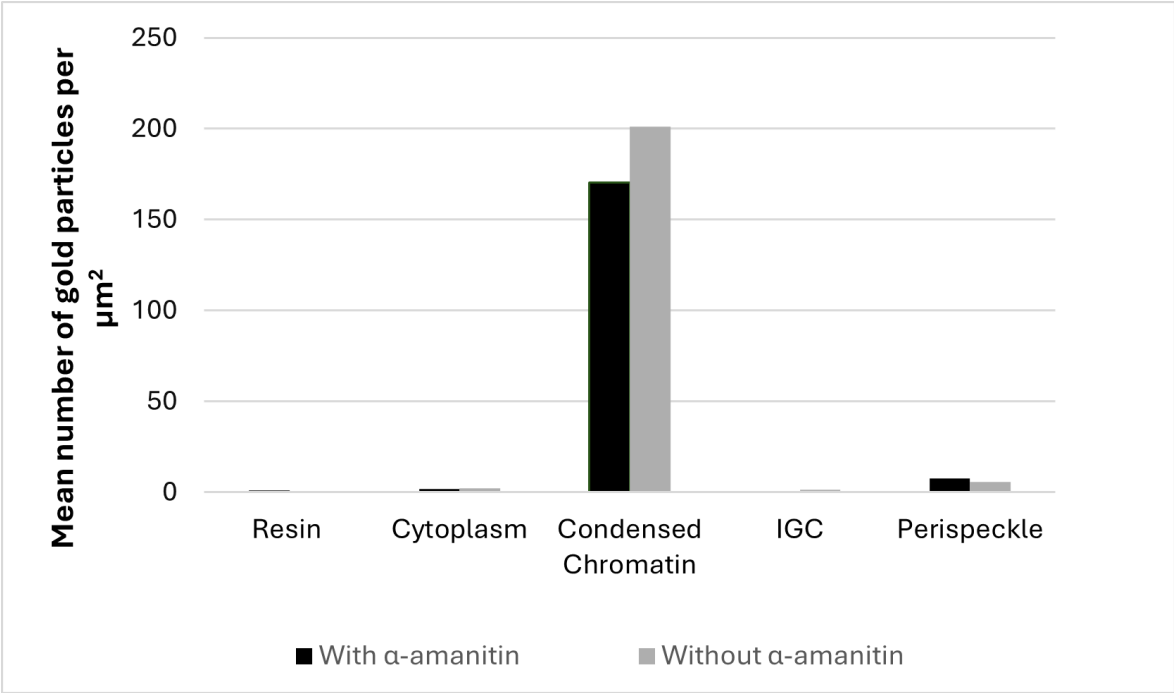


Figure 5

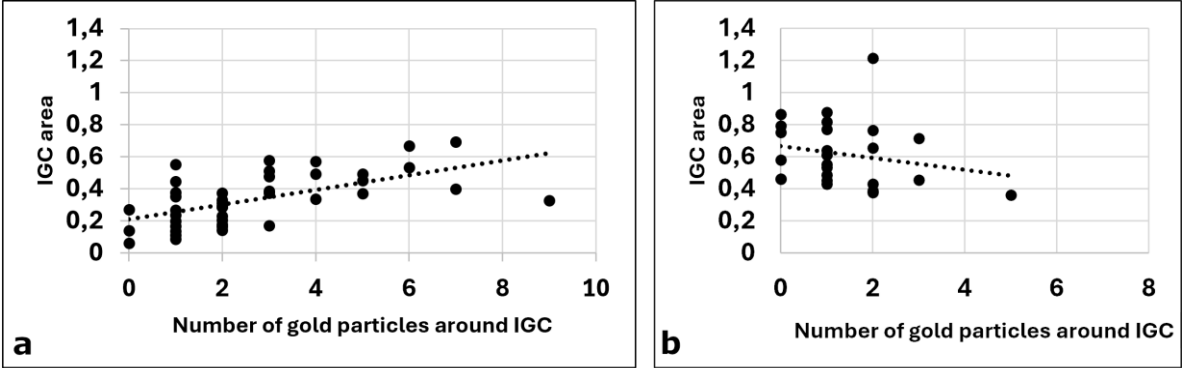


Figure 6

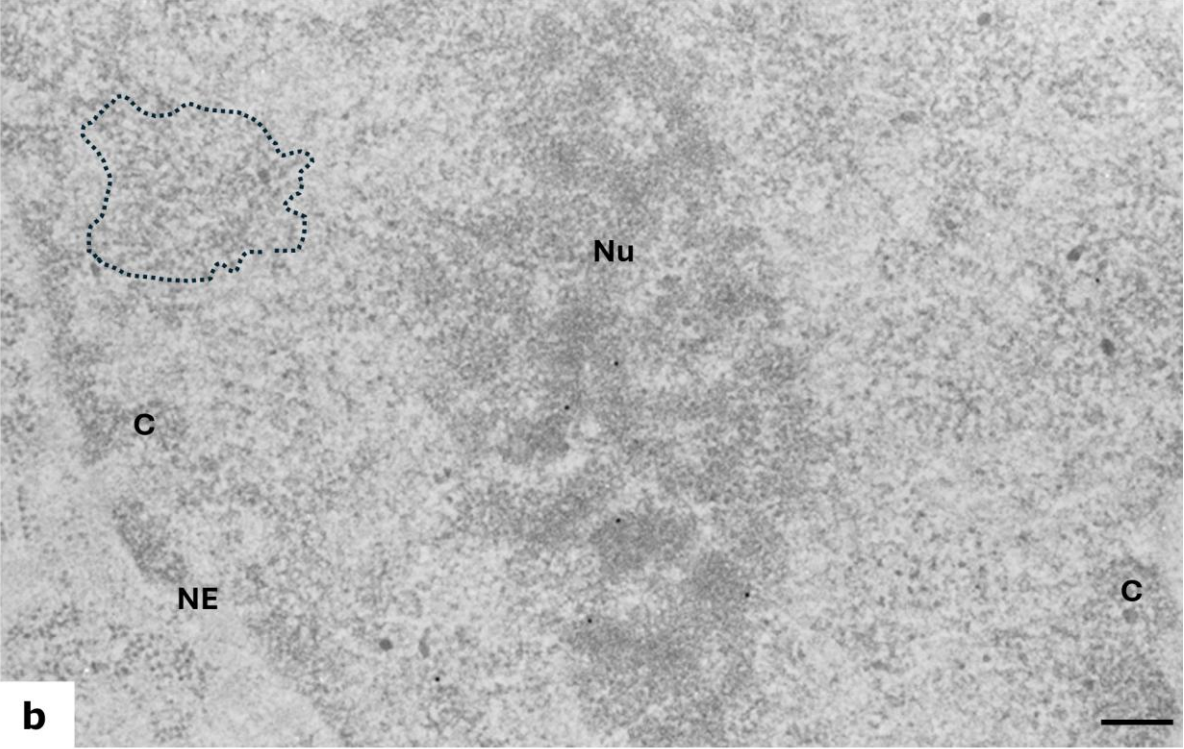
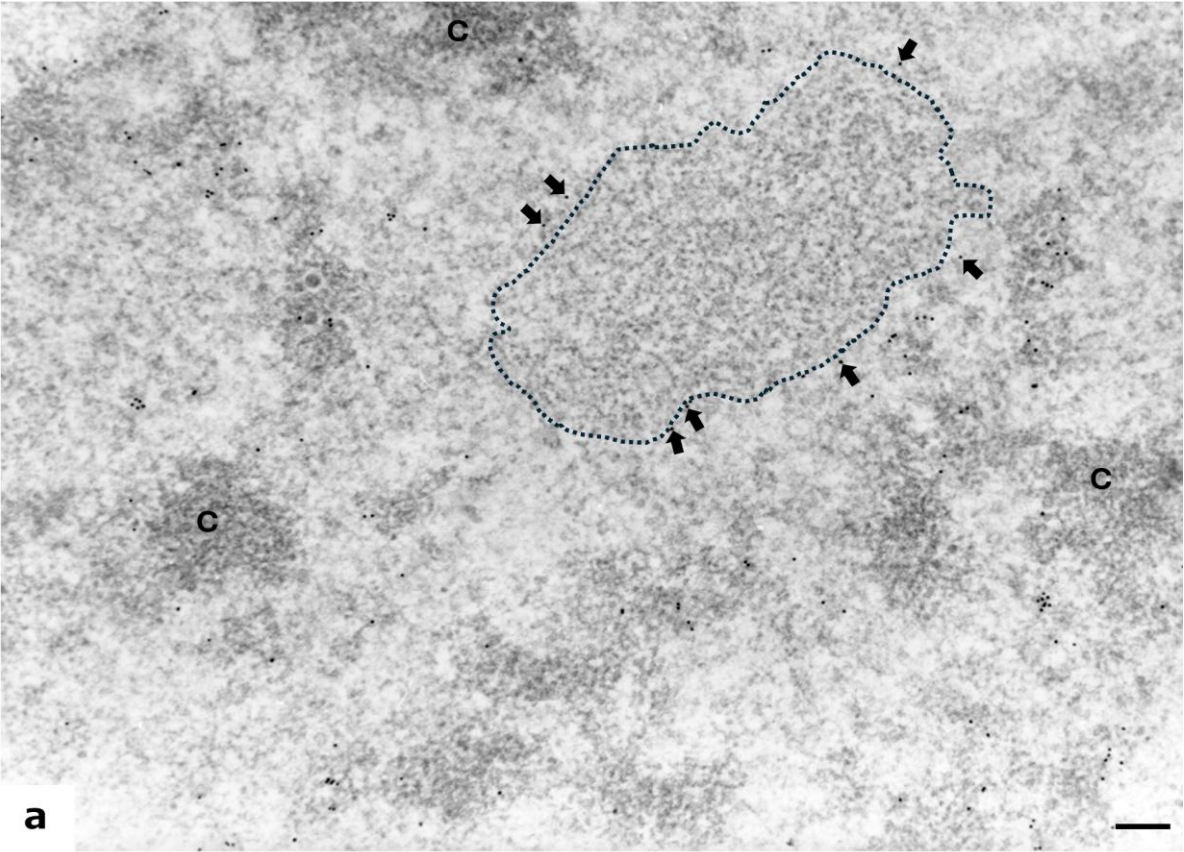


Figure 7

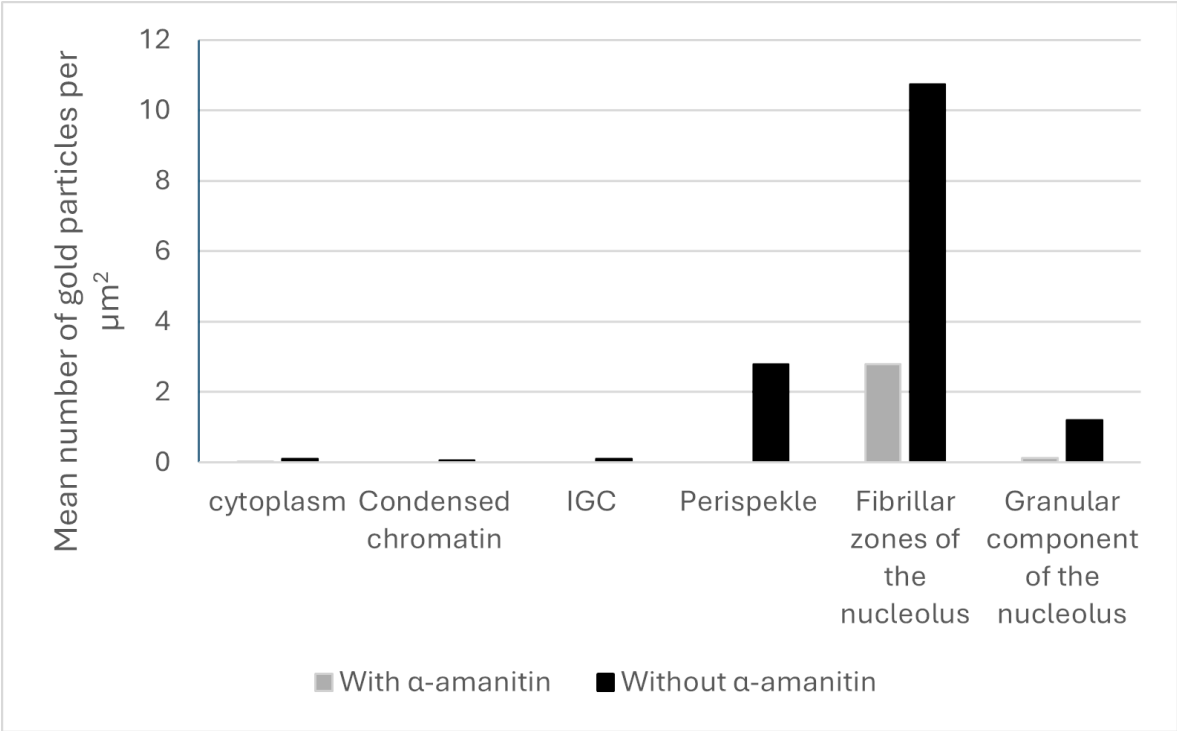


Figure 8

